

Nano-scale "Plasmon-Soliton"

Eyal Feigenbaum and Meir Orenstein*

Department of Electrical Engineering, Technion, Haifa 32000, Israel

Abstract

Formation of a novel hybrid-vector spatial plasmon-soliton in a Kerr slab embedded in-between metal plates is predicted and analyzed with a modified NLSE, encompassing the hybrid vector field characteristics. The soliton self-trapping in the lateral dimension is enhanced by the transverse plasmonic effect, yielding effective soliton dimensions of 100nm or less - representing the smallest reported optical soliton.

* Electronic address: meiro@ee.technion.ac.il

The downscaling of conventional photonic circuitry is bounded by a transverse dimension of $\sim\lambda/2$ (λ is the medium wavelength). This limitation can be alleviated by the incorporation of metals, giving rise to surface plasmon polaritons (SPP) [1,2]. Here we analyze a novel configuration where light is transversely tightly guided between two metal layers, and laterally self trapped by the Kerr effect. The plasmon polariton effect enables overcoming the $\lambda/2$ confinement limitation in both transverse and lateral dimensions. Moreover, the implementation of nonlinear self-trapping, rather than ordinary waveguiding, enables all-optical controlled interconnects, and relaxes the requirement for fabrication of in-plane nano-structures. The tight field confinement of our scheme is instrumental also for exhibiting such solitons with very small optical powers, which is further assisted by the expected small group velocity of the plasmon-soliton. In this letter we present for the first time both an analysis of TM spatial solitons, using the Non-linear Schrödinger Equation (NLSE), where the full vectorial field is considered, as well as the prediction and characteristics of nano scale SPP based solitons.

The underline mechanism for overcoming the regular diffraction limits when SPP waves are encountered is related to the fact that they are slow waves, namely their propagation momentum is larger than that of a plane wave propagating in the same dielectric. The specific setting of a dielectric layer enclosed by two metal layers, supporting SPP mode, is thus equivalent to a 2-dimensional subspace with reduced in-plan diffraction. The latter assists in exhibiting both linear [1] and nonlinear photonics with lateral light field dimensions substantially smaller than the wavelength. For the formation of "nano" – soliton – the reduced diffraction is instrumental also for the proper transformation from Maxwell equations to the NLSE of the envelope function. Only under reduced diffraction conditions – this transformation can take place at such small dimensions as detailed below.

The plasmon-soliton analysis starts by deriving a novel NLSE for TM modes nonlinearly laterally confined, taking into account the two electric field components, while the plasmonic effect will be introduced later via a metal cladding structure. An NLSE based analysis of TM solitons which are self trapped laterally (in-plane) by the Kerr nonlinearity, while confined transversely (vertical) by a slab waveguide structure, was never performed, with detailed consideration of the full vectorial nature of the field (to the best of our knowledge). This type of analysis is essential for the SPP based solitons which carry a substantial longitudinal electric field. Experimental reports of transversal guided solitons in slab waveguides addressed TE polarization [e.g. 3]. As for theory, most of the analysis was focused on (1+1)D solitons with nonlinearity that modifies the transverse guiding mode profile (or self sustained in a bulk nonlinear media), while invariant (infinite) in the lateral dimension [e.g. 4-8]. Neither included the full vector nature of the guided soliton, although some incorporated waveguiding effects in the transverse dimension, using a variation method [9].

In our structure - continuous waves are propagating in z direction, while being confined in the x direction (transverse) by slab waveguide layers and self-trapped by Kerr nonlinearity in y axis (lateral). For vanishing nonlinearity the structure supports TE and TM mode families, however, this distinction based on $\partial y=0$ is false when the nonlinearity sets in, resulting in self-trapping in y direction and the coupling of the TE/TM modes. Nevertheless, TE/TM based analysis is reasonable when the soliton width (Δy) is significantly larger than the mode width (Δx). (the x -axis field distribution enters the y -axis calculation as an effective parameter, similar to conventional prescriptions for temporal fiber solitons [10]).

The wave equation obtained from Maxwell equations by introducing Kerr type nonlinearity [8] is:

$$\nabla \times \nabla \times \bar{E} - k^2 \bar{E} = \frac{4n_2}{3n_0} k^2 \left[|\bar{E}|^2 \bar{E} + \frac{1}{2} (\bar{E} \cdot \bar{E}) \bar{E}^* \right] \quad (1)$$

Where $k=k_0 n_0$ is material k-vector with n_0 and n_2 the respective linear and nonlinear Kerr refractive indices. For TM modes $\partial_z E_z = \partial_x E_x$, thus the LHS of (1) is:

$$\nabla \times \nabla \times \bar{E} = -\nabla^2 E_x \hat{x} - \nabla^2 E_z \hat{z} \quad (2)$$

where the y-component is trivially satisfied. This implies that the wave equations for the two electric field components become identical, which is instrumental for the integrity of the soliton (otherwise each field component will evolve differently), as well as for the ability to employ a single scalar NLSE aligned with the field. Weak nonlinearity is assumed, thus a negligible effect is expected to the mode shape in the x-direction:

$$\bar{E} = \bar{E}_0(x) A(z, y) \exp\{j\beta z\} \quad \bar{E}_0 = E_x \hat{x} + E_z \hat{z} \quad (3)$$

\bar{E}_0 is the TM field distribution for vanishing nonlinearity, A a slowly varying envelope, and β the z propagation constant. Using the paraxial approximation along z (namely omitting A_{zz}), Eq. (1) becomes:

$$2j\beta \bar{E}_0 A_z + \left[(k^2 - \beta^2) \bar{E}_0 + \bar{E}_0'' \right] A + \bar{E}_0 A_{yy} + \frac{4n_2}{3n_0} k^2 \left[|\bar{E}_0|^2 \bar{E}_0 + \frac{1}{2} (\bar{E}_0 \cdot \bar{E}_0) \bar{E}_0^* \right] |A|^2 A = 0 \quad (4)$$

Multiplying (4) by \bar{E}_0^* and averaging over x yields a scalar wave equation for the amplitude A:

$$j2\beta A_z + \left[(k^2 - \beta^2) + \frac{I_2}{I} \right] A + A_{yy} + \frac{4n_2}{3n_0} k^2 \frac{I_3}{I} |A|^2 A = 0 \quad (5)$$

$$I = \int_{-\infty}^{+\infty} |\bar{E}_0|^2 dx; \quad I_2 = \int_{-\infty}^{+\infty} \bar{E}_0^* \bar{E}_0'' dx; \quad I_3 = \int_{core} \left\{ |\bar{E}_0|^4 + \frac{1}{2} (\bar{E}_0 \cdot \bar{E}_0) (\bar{E}_0^* \cdot \bar{E}_0^*) \right\} dx$$

The averaging operation is reasonable when the transverse (x) cross-section is smaller than the lateral (y). For a slowly varying amplitude ($a=A \exp\{-j(k^2 - \beta^2 + I_2/I)/(2\beta)z\}$) the NLSE is:

$$ja_z + \frac{1}{2\beta} a_{yy} + \frac{2n_2 k^2}{3n_0 \beta} \frac{I_3}{I} |a|^2 a = 0; \quad (6)$$

A first order soliton is a solution of this equation, with peak amplitude η and width Δy :

$$\Delta y \cdot \eta = \sqrt{3I / (16\pi^2 n_0 n_2 I_3)} \lambda_0 \quad (7)$$

λ_0 is free space wavelength. We normalize the average vertical intensity in the core to unity ($d^{-1} \int_{\text{core}} |E_0|^2 dx = 1$), thus η^2 is the soliton peak power.

For completeness we note that a similar derivation for TE modes indicates the deficiency of diffraction in the y direction. The LHS of (1) for TE mode ($\vec{E}_0 = E_y \hat{y}$) becomes:

$$\nabla \times \nabla \times E = \partial_{xy} E_y \hat{x} - (\partial_{xx} + \partial_{zz}) E_y \hat{y} + \partial_{zy} E_y \hat{z} \quad (8)$$

which for non cross-directional susceptibilities yields $\partial_y E_y = 0$ which manifests that solitons self trapped in the y direction cannot be supported by a TE mode while guided by the x layered structure.

We employ now the general results for TM modes to the gap SPP configuration, where a thin Kerr dielectric slab is sandwiched between two metal layers. This structure supports modes with cross-section much smaller than a wavelength. The modal field is effectively bounded to the gap in-between the metal layers, and can be reduced almost indefinitely with the thickness d without cutoff. Moreover, the "plasmonic" effect enables also the reduction of the lateral dimension in the transparent waveguide core [1]. In Fig. 1 the effective index dependence on the wavelength and gap width (d) is depicted for the even and odd transverse modes. Higher effective indices, thus smaller lateral solitons, are exhibited for symmetric modes, with smaller d -gaps and as the wavelength is reduced towards the asymptotic SPP wavelength ($\lambda_{\text{SPP}} = (1 + n_0^2)^{0.5} \lambda_{\text{plasma}}$).

For a non-plasmonic configuration, namely regular dielectrically cladded nonlinear slab, applying (7) yields a minimum of the effective transverse dimension for the spatial soliton

$(D_{\text{eff}}=(\Delta x \Delta y)^{0.5})$ obtained for a slab thickness of $\sim \lambda/2$ (see Fig. 2). When trying to enhance this soliton confinement by further increasing the intensity, the paraxial assumption breaks as the accumulated nonlinear phase becomes comparable to that of propagation - such that formal solitons are not a self solution of the configuration. However, for the metal embedded nonlinear slab – as verified below - the "plasmonic" effect is harnessed to overcome this minimum soliton width restriction.

Solving for a nonlinear dielectric sandwiched between two silver layers yields a closed form expression for the soliton width from (7). The effective mode size in a slab embedded in metal cladding is depicted in Fig. 2 (black) and compared to air cladded slab case (red). The "plasmonic" signature is evident: in contrast to the dielectric clad case – having a minimum of D_{eff} , in the plasmonic case - the effective size is reduced indefinitely with gap thickness and it is apparent that nano-scale dimensions below the diffraction limit ($D_{\text{eff}} < 100\text{nm}$) are achievable, (blue). As a precaution – we restrict the validity of our model to regions where $\Delta y \gg \Delta x$ (not satisfied in the dashed segments of the figure).

To asses correctly the plasmon-soliton solutions, the following should be memorized: First – the typical propagation length for highly confined SPP waves is limited to the micro scale regime due to metal losses, and it is this typical propagation length we expect for the plasmon-soliton as well; Second, we discuss here only solutions that are within the constrains of the analytical model – namely formal hybrid NLSE plasmon-solitons, however other and not less-interesting nonlinear wavepackets may exist under the conditions set by the plasmonic effect – which require more complex modeling (e.g. for higher intensity, lower wavelengths, similar transverse and lateral dimensions, rapidly varying envelop etc.).

Cross-sections of the plasmon-soliton field intensity are depicted in Fig 3. A plasmon-soliton excited by an input wavelength of 820nm is shown in Fig 3(a), for $\eta^2=700\text{KW}/\mu\text{m}^2$ and $d=40\text{nm}$. The plasmon-soliton has nano-scale effective width of $\sim 100\text{nm}$, while an all-dielectric slab-soliton, for the same peak power, has a minimal effective width which exceeds the diffraction limit ($D_{\text{eff}}=370\text{nm}$). Further more – the latter all dielectric soliton exhibits accumulation of nonlinear phase comparable to the linear phase of the optical carrier, which severely limits the soliton notion here. For the plasmon-soliton the metal losses results in a decay length of $\sim 11\mu\text{m}$, larger than the soliton length of $\sim 2.7\mu\text{m}$, which justifies the validity of using the notion of soliton. Checking the validity of our approximations – reaffirms both the paraxial approximation, as the soliton length is much higher than the wavelength of the carrier wave (440nm), as well as the TM assumption - inplane dimension ($\Delta y=250\text{nm}$) is substantially larger than the vertical one ($\Delta x=40\text{nm}$). We should note that even when both dimensions become comparable, the experience shows that TM analysis holds (e.g., see [1,2]).

As the wavelength is increased, the losses are reduced. In Fig. 3(b) the intensity cross-section of a plasmon-soliton is depicted, at the communications wavelength (1550nm). A sub-halfwavelength average width ($\sim 260\text{nm}$) is obtained with decay length of $30\mu\text{m}$.

As the wavelength is reduced towards λ_{SPP} , or alternatively increasing the gap width, the field is collapsing towards the interfaces, as elucidated in Fig 3(c) for gap width of $d=200\text{nm}$ at wavelength of 820nm. Enhanced gap width results also in reduced losses; $26\mu\text{m}$ decay length for the current example. Approaching further the SPP resonance (frequency-wise) or increasing further the gap width – generates effectively two coupled wavepackets – each on a one metal surface, which represents a much higher degree of confinement – however this case is not faithfully described by the analytical soliton model.

We derived a hybrid vector NLSE describing slab confined TM modes which are self trapped in the free (in-plan) dimension by the Kerr effect. A nonlinear slab sandwiched between metal layers supports a hybrid "Plasmon-Soliton", exhibiting high confinement in both transverse dimensions – lower than the conventional diffraction limit. In such structures, the losses will determine the useful propagation length of these solitons. A reach variety of additional ultra-confined nonlinear wavepackets, not conforming to the approximations used to derive the NLSE are yet to be explored.

Acknowledgements

We would like to acknowledge the Israel Ministry of Science and Technology for partial support of this research.

References

- [1] P. Grinberg, E. Feigenbaum, M. Orenstein, "2D Photonic Band Gap Cavities Embedded in a Plasmonic Gap Structure - Zero Modal Volume?," LEOS Annual Meeting, Australia (paper TuZ5) (2005).
- [2] F. Kusunoki, T. Yotsuya, J. Takahara, T. Kobayashi, Appl. Phys. Lett. **86**, 211101 (2005).
- [3] J.S. Aichison, Y. Silberberg, A.M. Weiner, D.E. Leaird, M.K. Oliver, J.L. Jackel, E.M. Vogel, P.W.E. Smith, J. Opt. Soc. Am. B **8**, 1290 (1991).
- [4] R.Y. Chiao, E. Garmire, C.H. Townes, Phys. Rev. Lett. **13**, 479 (1964).
- [5] D. Mihalache, M. Bertolotti, C. Sibilia, Progress in optics **27**, 227 (1989).
- [6] Y. Chen, Phys. Re. A **44**, 7524 (1991).
- [7] E. Granot, S. Strenklar, Y. Isbi, B.Malomed, A. Lewis, Opt. Lett. **22**, 1290 (1997).
- [8] A. Ciattoni, B. Crosignani, P. DiPorto, A. Yariv, J. Opt. Soc. Am. B **22**, 1384 (2005).
- [9] R.A. Sammut, C. Pask, Q.Y. Li, J. Opt. Soc. Am. B **10**, 485 (1993).
- [10] C.R. Menyuk, J. Eng. Math. **36**, 113 (1999).
- [11] E.D. Palik, *Handbook of optical constants of solids*, (Academic, San-Diego, 1998)

Figure Captions

FIG. 1. n_{eff} of transverse modes in between metal plates vs. wavelength: even (bold-black) and odd (dashed-blue) modes, single surface mode (dashed red). $\lambda_{\text{plasma}}=137\text{nm}$, $n_0=1.5$.

FIG. 2. D_{eff} vs. d . Nonlinear Kerr slab embedded in metal (black) and air (red). $\lambda_{\text{plasma}}=137\text{nm}$, $\lambda_0=820\text{nm}$, $n_0=1.5$, $n_2=4\text{E-}15 \text{ cm}^2/\text{W}$, Intensities (η^2) are given in $\text{KW}/\mu\text{m}^2$ on curves. Diffraction limit and the nano-regime limit are denoted by green and dashed green lines accordingly.

FIG. 3. Plasmon-soliton intensity cross-section. Glass: $n_0=1.5$, $n_2=4\text{E-}15 \text{ cm}^2/\text{W}$. silver plates [11]. (a) $\lambda_0=820\text{nm}$, $d=40\text{nm}$, $\epsilon_M = -30.2-i1.6$, $\eta^2=700\text{KW}/\mu\text{m}^2$, $D_{\text{eff}}=100\text{nm}$. (b) $\lambda_0=1550\text{nm}$, $d=100\text{nm}$, $\epsilon_M = -103.5-i10$, $\eta^2=700\text{KW}/\mu\text{m}^2$, $D_{\text{eff}}=266\text{nm}$. (c) $\lambda_0=820\text{nm}$, $d=200\text{nm}$, $\eta^2=600\text{KW}/\mu\text{m}^2$, $D_{\text{eff}}=270\text{nm}$.

Figure 1

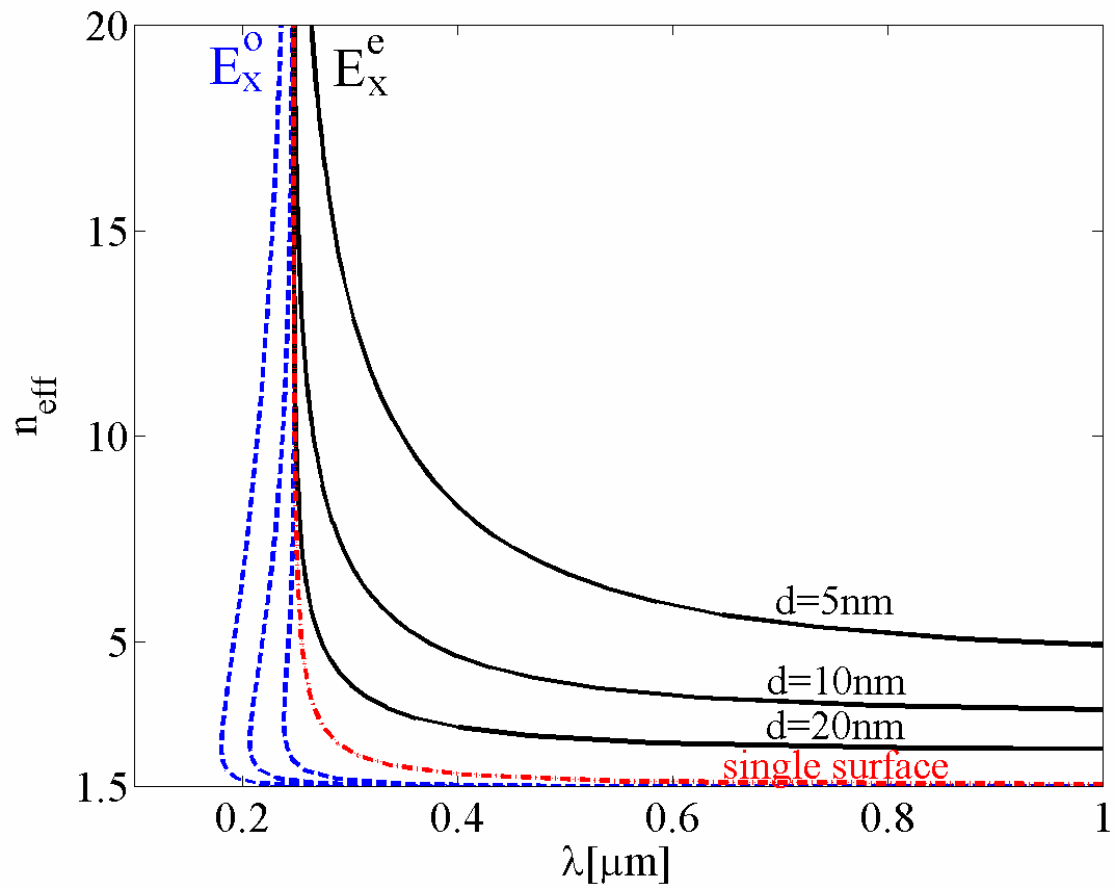


Figure 2

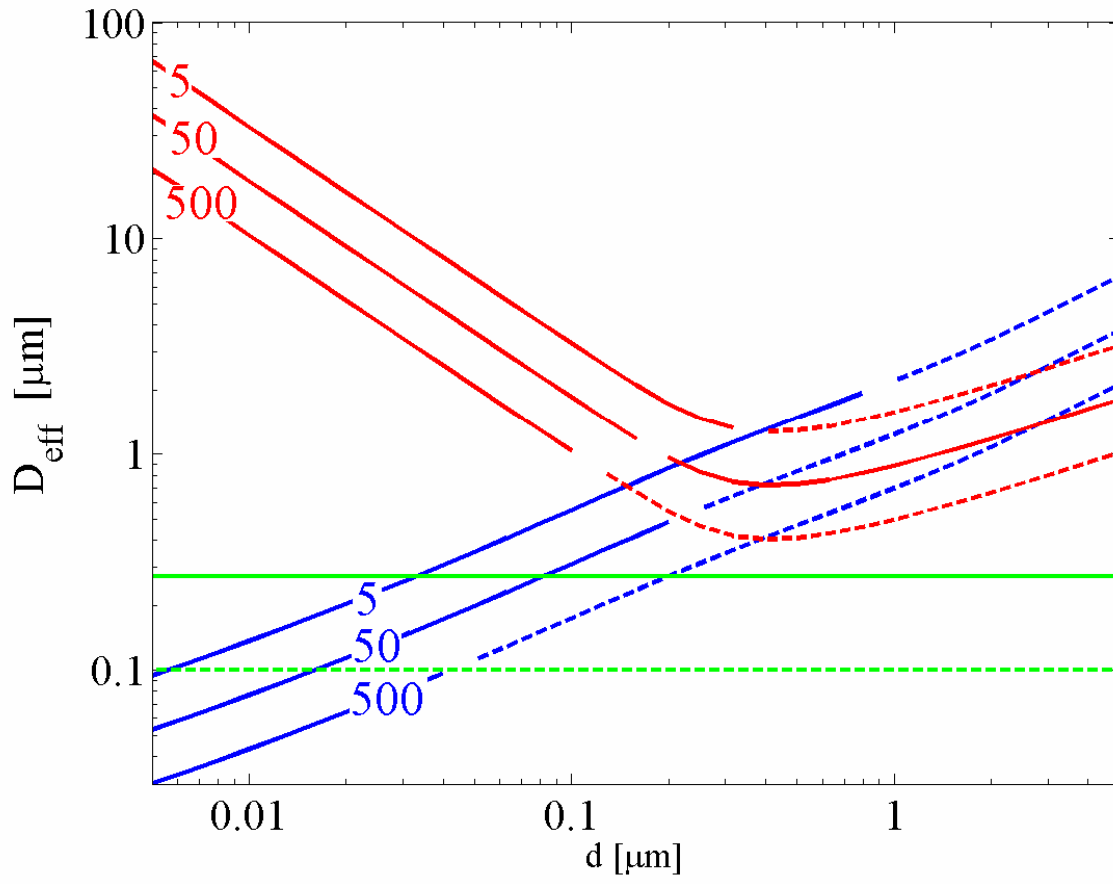


Figure 3(a)

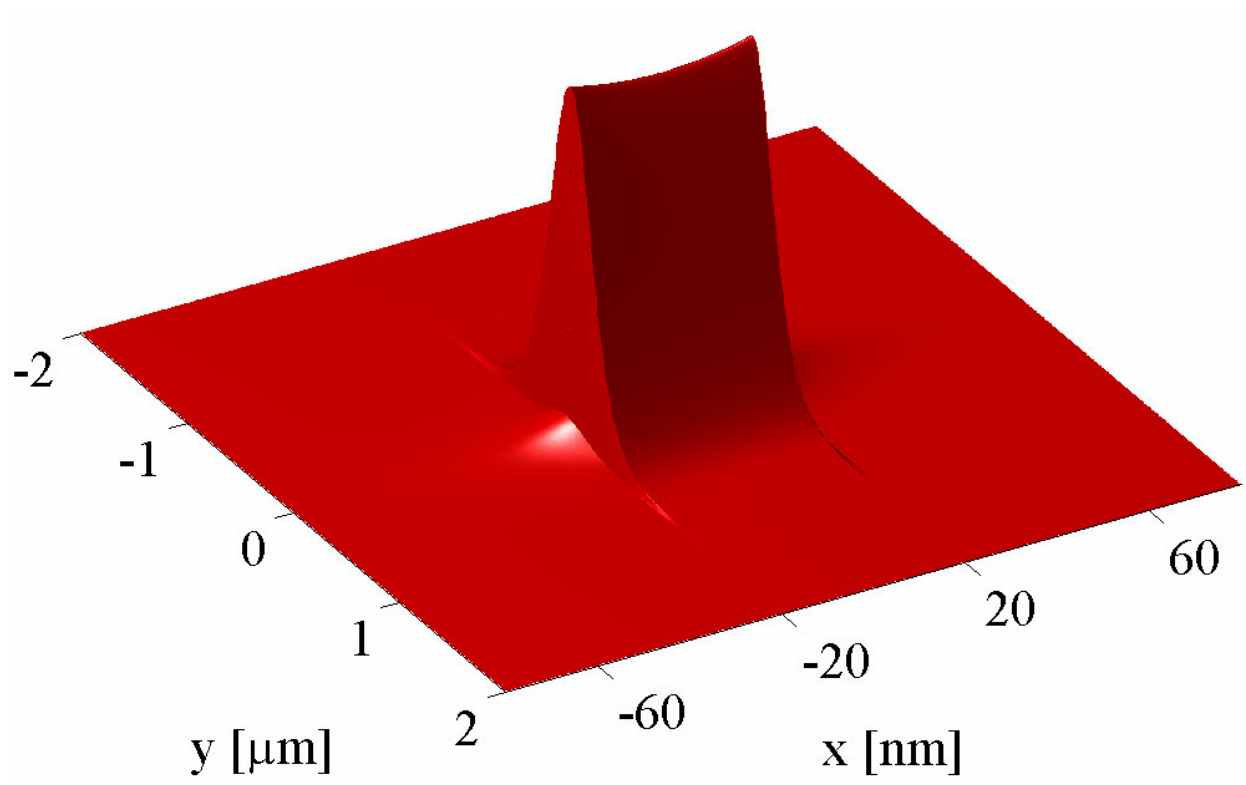


Figure 3(b)

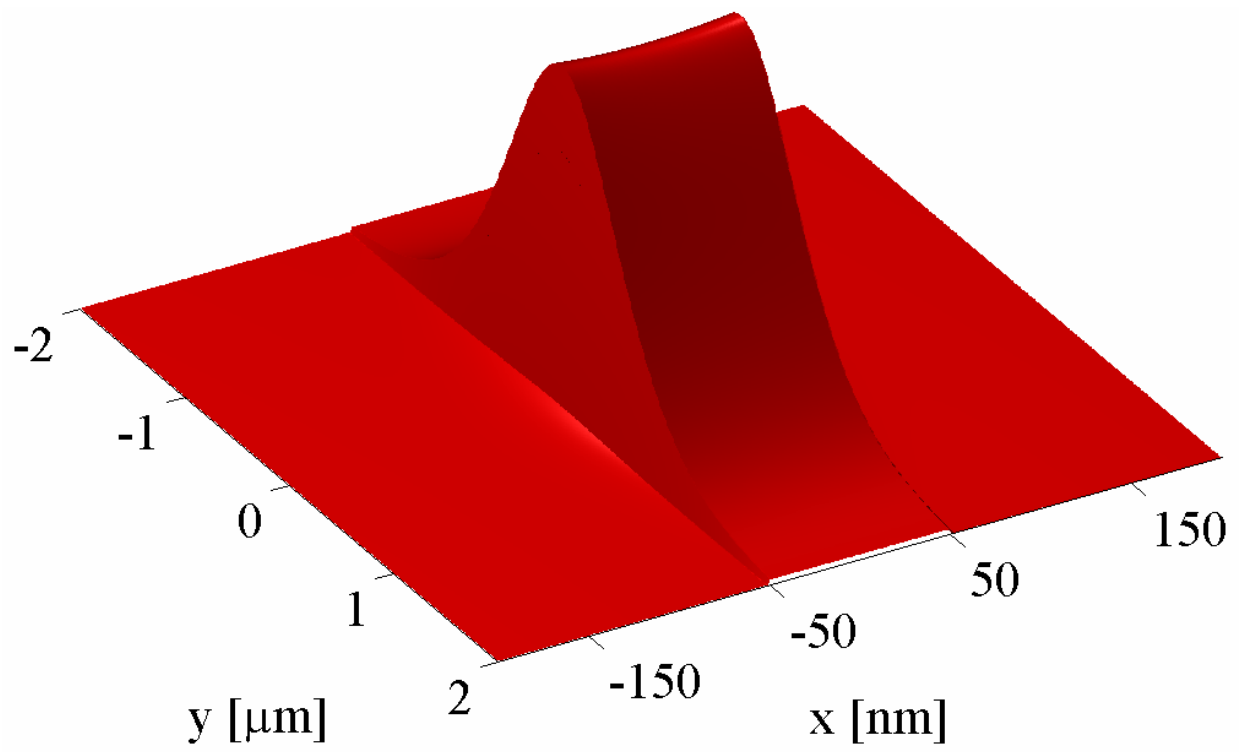


Figure 3(c)

